Double photoionization of Mg studied by electron-electron coincidence experiments

E. Sokell[1], P. Bolognesi[2]A. Kheifets[3], Igor Bray[4], S Safgren[1], and L. Avaldi[2]

[1] School of Physics, UCD Science Centre, Belfield, Dublin 4, Ireland
[2] CNR-Istituto di Metodologie Inorganiche e dei Plasmi, Area della Ricerca di Roma1, 00015 Monterotondo Scalo, Italy
[3] RSPE, The Australian National University, Canberra ACT 0200, Australia
[4] ARC Centre for Matter-Antimatter Studies, Curtin University, WA 6845 Perth, Australia

Abstract

The double photoionization (DPI) of Mg to the $Mg^{2+}(3s^{-2})$ state has been studied by photoelectron-photoelectron coincidence experiments at a photon energy corresponding to the excitation of the 2p→3d resonance. The equal energy sharing (E_1=E_2=16.4 eV) as well as the complementary unequal energy (E_1↔E_2=10.4↔22.4 eV) sharing kinematics have been investigated. The experimental angular correlation patterns are compared to CCC calculations in which the resonant process has been incorporated. From the experimental results the symmetrised gerade and ungerade amplitudes have been obtained. The gerade amplitude in the case of the equal energy sharing shows a strong deviation from the Gaussian ansatz and supports the parametrization by a di-gaussian function, whose parameters are determined by the oscillation in the coordinate space of the target radial wave function. The triple differential cross Sections in the kinematics where one photoelectron is detected at a fixed direction of 90° with respect to the polarization direction of the radiation have been also investigated by extensive simulations which take into account the experimental acceptances as well.

PACS : 32.80.Fb

I. Introduction

The study of emission of two electrons from an atom by absorption of a single energetic photon, process referred to as atomic double photoionization (DPI), has attracted a lot of interest because it provides unique information on the electron-electron interaction . Experiments, in which either both the photoelectrons after angle and energy selection or one photoelectron and the recoil ion are detected in coincidence, provide the most detailed information on the process via the measurement of the triple differential cross Section $d^3\sigma/dE_1 d\Omega_1 d\Omega_2$ (TDCS). The study of DPI in the simplest two-electron system, the He atom, challenged for a long time both experimentalists and theorists and showed that the dynamics of the electron pair is strongly constrained by its own symmetry and the Coulomb repulsion. As far as the experiments are concerned, different approaches to circumvent the low value of the double ionization cross Section have been devised and nowadays a broad set of data from threshold up to 450 eV above it in different energy sharing conditions of the electron pair are available [1]. On the theoretical side, DPI which is the archetypal example of a three-body Coulomb problem, represents a non-separable problem, which cannot be given exact analytical solutions. Methods in quantum mechanics have been developed to give nearly exact solutions for the He three-body ground and excited discrete states. However the high doubly excited states and the double continuum states had to wait for the development of powerful computers to be accessible by numerical calculations. These methods have been reviewed firstly by Briggs and Schmidt in [2] and, more recently, by Malegat [3]. The joint experimental and theoretical efforts have lead to a good understanding of the DPI process, at least as far as the two-electron He system is concerned.

Alkaline-earth-metal atoms (Be, Mg, Ca, Sr) are "quasi two-electron" systems and represent the most suitable candidates for extending the investigation of DPI beyond He. In these atoms, the outer valence shell is well separated from the rest of the atom. Thus, in the DPI of the two outer shell electrons, the inner and sub-valence electrons can be treated as "spectators". With this assumption, the DPI process in alkaline-earth-metal atoms is similar to that in He except for a different radial structure of the target *ns* orbital and the influence of the distorting potential of the core on the departing photoelectrons. The theoretical double photoionization cross Section of Be and heavier alkaline-earth-metal atoms have been calculated within several theoretical schemes [4-10]. Recently Kheifets and Bray [11] made a systematic investigation of Be, Mg and Ca to elucidate the role of the ground- and final-state correlations. Their results showed that the narrowing of the angular correlation is related to the shrinking of the *ns* orbital in the momentum space. More recently [12] a strong effect of the target electronic structure was observed in the calculation of the angular correlation pattern in the two-electron continuum following L-shell double photoionization. It has

been shown that (i) for a given symmetry of the electron pair the DPI angular correlation mimics the angular distribution of an *e*-impact ionization of the corresponding ion and (ii) the amplitudes of these processes are strongly determined by the radial extent and the oscillations of the target orbital of the singly charged ion.

On the experimental side, the ratio of the double to single photoionization cross Sections, σ^{2+}/σ^{+}, of alkaline-earth-metal atoms has been measured for Be [13], Mg [14,15], Ca and Sr [16]. Unfortunately, the low target density achievable in metal vapor beams adds up to the low value of the DPI cross Section. Thus, even at the third generation synchrotron radiation sources, the measurement of the TDCS is a hard task and, to our knowledge, only a TDCS in Ca has been reported in the non-resonant condition at an excess energy of 25 eV [17]. Fortunately, the presence of np→n'd resonances in the double continuum has made possible the measurement of the TDCS in a few other cases [18-21]. On one hand these resonances enhance the photoabsorption cross Section and therefore the emission of the two electrons. However, on the other hand, they may affect the shape of the TDCS because the intermediate excited state populates the double continuum via the ejection of two-electrons [22]. Indeed some "anomalous" observations in the TDCS of Ca and Sr measured at the 3p→3d and 4p→4d resonances, respectively, have been interpreted as a signature of this indirect process. These anomalies consisted of extra-lobes in the TDCS with respect to the double photoionization of He, in particular, when one electron is measured at 90° with respect to the polarization axis of the incident radiation.

In this work, we have measured the TDCS for the DPI of Mg at 55.49 eV, which corresponds to the excitation of the 2p→3d resonance, in the equal energy sharing conditions (E_1=E_2=16.4 eV) and in two complementary unequal energy sharing conditions (E_1= 10.4 eV, E_2=22.4 eV), where the kinetic energy of the photoelectrons $E_1 \leftrightarrow E_2$ has been exchanged. The TDCS has been also calculated by incorporating semi-empirically the effect of the resonant excitation in the convergent close-coupling (CCC) [23] formalism. A subset of the data taken in the equal energy sharing condition has been recently presented in a shorter Letter format [24].

The paper is organized as it follows. In Sections II and III, respectively, the information about the experimental set-up and procedures, and the details of the theoretical model are presented. The experimental results and their comparison with the theoretical predictions are shown and discussed in Section IV. In the same Section, we also address the specificity of the kinematics with a fixed electron measured at 90° with respect to the polarization axis of the incident radiation. Finally, conclusions are drawn in Section V.

II. Experimental

The experiments have been performed using the electron-electron multicoincidence end-station [25] at the Gas Phase Photoemission [26] beamline of the Elettra storage ring, where an undulator of period 12.5 cm, 4.5 m long produces completely linearly polarized radiation in the photon energy range 13-1000 eV with a typical resolving power of 10.000. In the present case, at the chosen photon energy hv= 55.49 eV, the energy resolution was degraded to about 150 meV in order to increase the photon flux. The vacuum chamber hosts two independent turntables, holding respectively three and seven electrostatic hemispherical analyzers spaced by 30° of each other. The three spectrometers of the smaller turntable are mounted at angles of 0°, 30° and 60° with respect to the polarisation vector of the light $\boldsymbol{\varepsilon}=\varepsilon\mathbf{x}$ and they have been used to measure the 'fixed electron', labelled 1, in the perpendicular plane. The larger turntable rotates in the plane perpendicular to the direction, **z**, of propagation of the incident radiation, and its seven analysers have been used to measure the angular distribution of the correlated electron, labelled 2, of complementary energy in order to fulfill the energy balance $E_1+E_2=hv-I^{2+}$. The ten analyzers have been set to detect electrons of kinetic energy $E_1= E_2=16.4$ eV in the equal energy sharing experiment, and $E_1= 10.4$ (22.4) eV, $E_2=22.4(10.4)$ eV in the two complementary unequal energy sharing experiments. The energy resolution and the angular acceptance in the dispersion plane of the spectrometers were $\Delta E/E_{1,2}$ = 0.03 eV and $\Delta\vartheta_{1,2} = \pm 3°$, respectively. The relative angular efficiency of the ten analyzers has been established and checked by measuring the photoelectron angular distributions for the photoionization Mg 2p and Ne 2p, with well known asymmetry parameters at the same excess energy above their respective ionization thresholds [27,28]. The same efficiency correction has been assumed for the coincidence measurements. The validity of this assumption was tested by measuring the coincidence yield at two positions of the larger turntable, which overlap the two analysers nearby. Therefore, all the experimental data are internormalized and can be reported on the same relative scale. This can be checked by observing that the same coincidence yield is measured for different configurations of the spectrometers, obtained by the interchange of energies and angles, which correspond to the same kinematics [29].

The metal vapour source is collinear with the photon beam, which passes through the hollow core of the source before interacting with the atomic beam. As in Ross and West [30], two thin-walled stainless steel tubes are mounted on the base and the heater wires are held within these two tubes.

The crucible, which holds the metal charge, is basically made by two co-axial cylinders which are welded together at one end. A distinctive feature of this crucible is that it is possible to have any number of apertures drilled in the closure piece and pointing to the interaction region. The number of apertures used, six in the present experiments, thereby increases the atom density at the interaction region. Facing the oven, the relatively closed interaction region provided by a copper cylinder coaxial with the photon beam and cooled to about 0°C traps the vapour beam, shielding the set-up and preventing its contamination. Suitable holes on the two bases of the cylinder allow the photon beam to pass through, ending up on the photodiode, where its intensity is monitored throughout the experiments. On the lateral surface of the cylinder, three 1cm holes for the fixed analysers and a large slot of 230° for the rotatable analysers allow the photoelectrons to leave the interaction region to be detected. In addition, an independent hypodermic needle is allowed in the interaction region, pointing about 2 cm away from the vapour beam to prevent blockage, and is used to admit rare gases in the interaction region for tuning and calibration purposes. The oven has been operated with a temperature setting of 410 and 470°C for the bottom and top parts of the crucible, respectively. An accumulation time of about 3 hours per point was necessary to reach the present accuracy in the experimental results.

III. Theory

The two-electron CCC formalism cannot tackle resonant processes *ab initio*. In the non-resonant DPI process from the valence $3s^2$ shell of Mg, the role of the $2p \rightarrow \varepsilon d$ transition was found insignificant as was confirmed by calculating single photoionization cross-Sections by the CCC and RPA methods, the latter with the full account of the inter-shell $3s^2$ and $2p^6$ correlation [11]. On the other hand, the resonant process lies at the heart of the resonant TDCS measurement. So it should be incorporated into the CCC formalism semi-empirically. In doing so, we note that the dipole matrix element varies near the resonance as [31]

$$D(\omega) = \frac{q+\varepsilon}{i+\varepsilon} D_0 \cong -iqD_0 \qquad (1)$$

at $\omega \approx \omega_0$ and $\varepsilon \approx \varepsilon_0$. Here $\varepsilon = (\omega-\omega_0)/(\Gamma/2)$ is the photon energy counted from the resonance and measured in units of its width Γ, q is the profile (Fano) index and D_0 is the matrix element in the

absence of the resonance. For the 2p→3d resonance in Mg, the profile index q≈–50 [32]. Eq. (1) leads to the Fano formula for the cross-Section [33]

$$\sigma(\omega) = \frac{(q+\varepsilon)^2}{1+\varepsilon^2}\sigma_0 \cong q^2\sigma_0 \qquad (2)$$

Photoionization of the valence $3s^2$ of Mg leads to various ns^+ ionic states of Mg^+. This direct photoionization process is illustrated by the left diagram in Figure 1. The resonant process (right diagram) involves the virtual 2p → 3d excitation in the $2p^6$ shell and results in the same final state. In principle, the resonance will be present in all energetically accessible final ns^+ channels, not only in the lowest $3s^+$ ionic state. The overlap of the non-orthogonal 3s atomic state and ns^+ ionic states is shown by the black dot on the graphs. However, each channel will have its own profile index, which is not known from experiment and are hard to calculate *ab initio*. So we ignore these resonances except in the ground ionic state, which makes the strongest contribution.

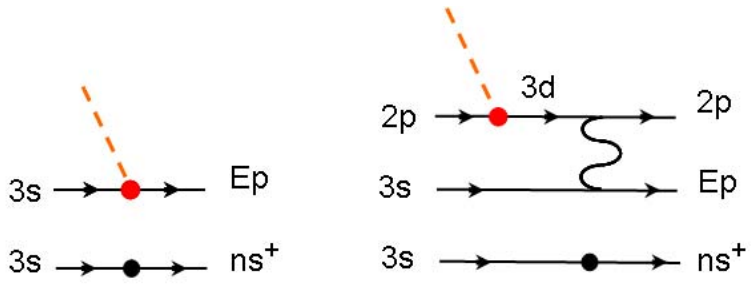

Figure 1 Diagrammatic representation of the direct (left) and resonant (right) photoionization processes in the valence $3s^2$ shell of Mg. The horizontal lines visualize electrons, the dashed line represents the photon and the wavy line exhibits the Coulomb interaction. The time propagates from left to right.

IV. Results and discussion

A.-Results

The experimental results, as well as the CCC calculations in the case of the equal energy sharing (E_1=E_2=16.4 eV) kinematics are shown in Figure 2 for three fixed reference angles ϑ_1=0, 30 and 60°. At all ϑ_1 the TDCS shape displays a node at ϑ_{12}=180° as expected by the singlet odd character of the double continuum wave function. At ϑ_1 =0° theory predicts two lobes of equal intensities, while at ϑ_1=30 and 60° the TDCS is mainly concentrated in one structure with some minor features: a small lobe at about 230° and a non-vanishing cross Section at about 100° at ϑ_1=30°, a series of three small lobes at ϑ_1=60°. The quality of the data does not allow to resolve properly all these features, but the general trend is in fair agreement with the predictions. At all ϑ_1 the additional feature (see arrows in Figure. 2) predicted in the main lobe, cannot be discerned in the experimental data. As far as the comparison with the double ionization of He in equal energy sharing at similar excess energy [34,24] is concerned, one sees that the Mg TDCS share with He the node at ϑ_{12}=180°, but the lobes in Mg are significantly narrower and the relative intensity and number of minor lobes at ϑ_1= 30° and 60° are different.

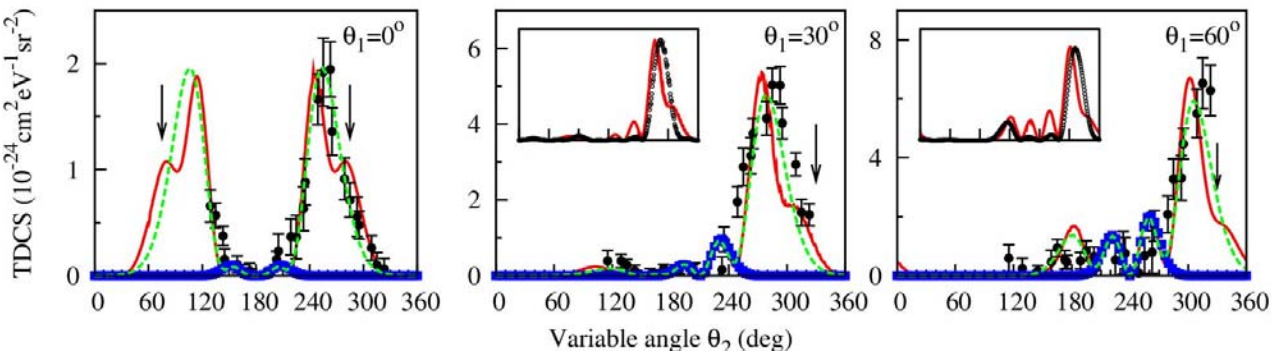

Figure 2. TDCS of Mg in equal energy sharing (E_1=E_2=16.4 eV) kinematics for three fixed reference angles ϑ_1=0, 30 and 60°. The resonant CCC calculation divided by the factor q^2 (red solid line) is fitted with the Gaussian ansatz eq.(5) (blue squares) and di-Gaussian parameterization eq. (6) (green dashed line). The non-resonant CCC calculation (scaled to the resonant CCC calculation) is shown on the inset with the black dots. The experimental TDCS (shown with error bars) have been rescaled to CCC (see text).

As the three TDCS were measured simultaneously, they can be reported on the same relative scale of intensity. A common scaling factor between theory and experiment has been used for the TDCS of Mg at ϑ_1=30 and 60°, while the theory appears to overestimate the experiment by a factor 2.2 at ϑ_1=0°. Similar variation of the scaling coefficients by a factor of 1.6 was required for He [24], which indicates the level of agreement between the present theory and experiment that we may expect. The non-resonant CCC calculations are shown in the inset of the figures, where they are compared to the ones including the resonance. For this purpose, the two calculations are scaled in a way that the maxima match in each figure. The non-resonant CCC displays the same narrowing of the lobes and presence of extra features in the TDCS, but for the ones indicated by the arrows in Figures 1. The absolute cross Section is about a factor four lower than in the calculations including the resonance (divided by the q^2 factor) and the main lobes have an intensity enhanced with respect to the other features.

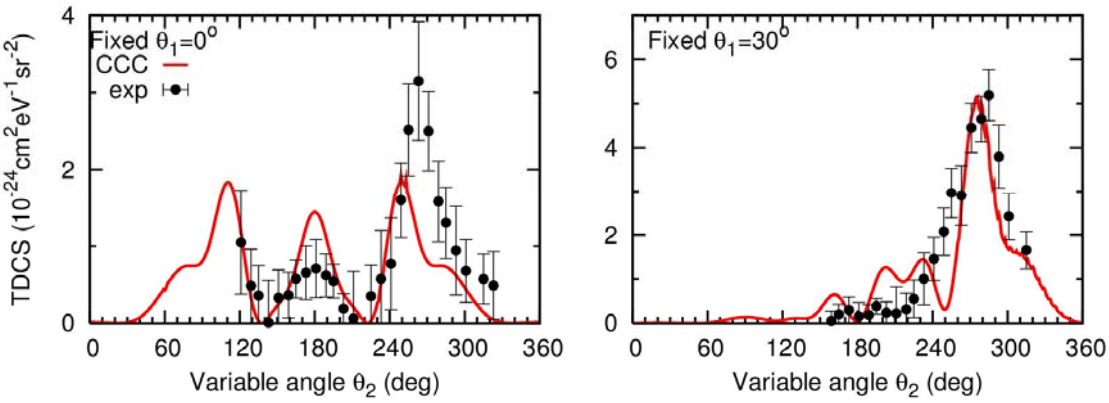

Figure 3a. TDCS of Mg in unequal energy sharing (E_1=10.4 eV, E_2=22.4 eV) kinematics for two fixed reference angles ϑ_1=0, and 30°. The experimental TDCS (shown with error bars) have been rescaled to CCC(red solid line) (see text)

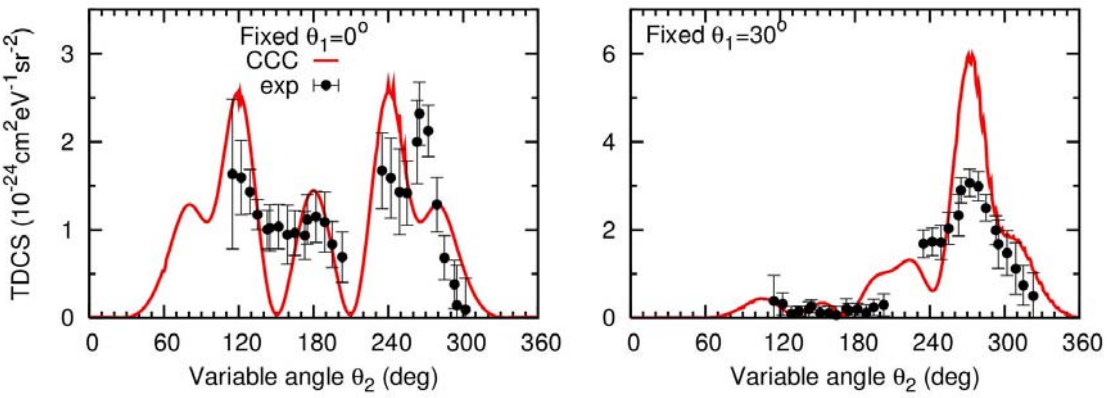

Figure 3b. TDCS of Mg in unequal energy sharing (E_1=22.4 eV, E_2=10.4 eV) kinematics for two fixed reference angles ϑ_1=0, and 30°. The experimental TDCS (shown with error bars) have been rescaled to CCC(red solid line) (see text).

The experimental results for the unequal energy sharing kinematics E_1=10.4 eV and E_2=22.4 eV and the complementary kinematics where E_1 and E_2 are exchanged, as well as the corresponding CCC calculations are shown in Figure 3a and b, respectively, for the fixed reference angles ϑ_1=0 and 30°. A common scaling factor between theory and experiment has been used for all these plots. In both kinematics, the theoretical TDCS at ϑ_1=0° are formed by three main lobes, with the side ones characterized by a double structure, while the TDCS at ϑ_1=30° display a main feature and a series of minor lobes. The absolute value of the TDCS increases when ϑ_1 increases from 0 to 30° in both the complementary kinematics, and the TDCS in the two side lobess at ϑ_1=0° is smaller by a factor of 15-20% when the electron measured at a fixed angle is the slower one. The experimental results are quite consistent with the predictions, the main discrepancies being in the relative intensity of the side lobes at E_1=10.4 eV and ϑ_1=0°, a shift of about 20° in the side peak at ϑ_1=0° in both complementary kinematics and the relative intensity of the different features at E_1=22.4 eV and ϑ_1=30°.

B. Discussion

By considering the invariance with respect to the rotation around the polarization direction of the incident radiation and the general properties of the spherical harmonics, the TDCS can be written in a way that allows full separation of the geometrical factors and the dynamical parameters, as shown in a very general way by Briggs and Schmidt [2]. This leads to a parametrization of the TDCS

which is particularly useful because it can be easily linked to the experimental observations. In the case of an incident radiation that propagates along the z axis and is fully linearly polarized along the **ε**=ε**x** axis the TDCS can be written as

$$TDCS(E_1, E_2, \vartheta_{12}) \propto \left| a_g(E_1, E_2, \vartheta_{12})(\cos\vartheta_1 + \cos\vartheta_2) + a_u(E_1, E_2, \vartheta_{12})(\cos\vartheta_1 - \cos\vartheta_2) \right|^2 \quad (3)$$

where ϑ_{12} is the relative angle between the directions of emission of the two photoelectrons . The complex amplitudes a_g and a_u are respectively symmetric and antisymmetric relative to the exchange of E_1 and E_2. The ϑ_{12} and E dependence of these amplitudes includes all the physical information on the dynamics of the process, i.e. the effects of the electron–electron and electron–residual ion interactions.

Under the equal energy sharing condition a_u=0 and the TDCS is determined by the symmetric, or gerade, amplitude

$$TDCS(E_1, E_2, \vartheta_{12}) \propto \left| a_g(E_1, E_2, \vartheta_{12})(\cos\vartheta_1 + \cos\vartheta_2) \right|^2 \quad (4)$$

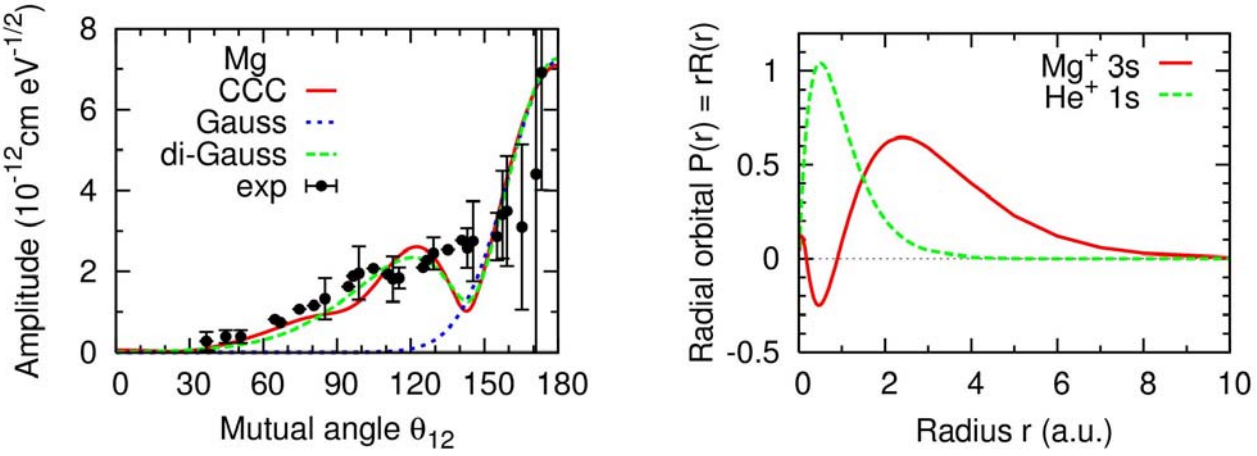

Figure 4. (*left*) The symmetric gerade amplitudes of DPI of Mg at $E_1 = E_2 = 16.4$ eV is drawn as function of the mutual photoelectron angle ϑ_{12}. The full CCC calculation (red solid line) is fitted with the Gaussian ansatz eq. (5) (blue dashed line) and di-Gaussian parameterization eq. (6) (green dashed line). The Mg amplitude extracted from the experimental TDCS is shown with error bars. (*right*) The radial orbitals *P(r) = rR(r)* for Mg^+ 3s (red solid line) and He^+ 1s (green dashed line).

The Mg amplitude extracted from the experimental TDCS is shown with error bars in figure 4, where it is also compared with the amplitude predicted by CCC. The comparison between the

theoretical and experimental amplitudes is quite satisfactory, although the quality of the data hampers a clear observation of the predicted minimum in the amplitude.

Based on the Wannier-type theories [35], in which the angular variation near the Wannier saddle decouples from the radial motion and can be described by the ground-state wave function of a harmonic oscillator, the symmetric amplitude a_g has been represented by a Gaussian function,

$$\left|a_g\right| = A\exp\left[-2\ln 2\left(\vartheta_{12}-180\right)^2/\Delta\vartheta^2\right] \equiv G(A,\Delta\vartheta,\vartheta_{12}) \quad (5)$$

where $\Delta\vartheta$ is the correlation width. The Gaussian ansatz has been found a useful approximation to describe the symmetric amplitude of the double photoionization of He up to an excess energy of 80 eV [36]. The central portion of the Mg amplitude, near the mutual photoelectron angle ϑ_{12}=180°, can be represented by the Gaussian ansatz, but the fringes of the Mg amplitude cannot. Indeed, the whole of the Mg amplitude can be better described by the di-Gaussian parametrization proposed in [37]

$$a_g = G(A_1,\Delta\vartheta_1,\vartheta_{12}) + e^{i\phi}G(A_2,\Delta\vartheta_2,\vartheta_{12}) \qquad (6)$$

The complex phase factor represents the interference of the two Gaussians. The five constants $A_{1,2}$, $\Delta\vartheta_{1,2}$ and φ are used as fitting parameters. As was argued in [37], the Gaussian width may be linked to the radial extent of the target orbital of the singly charged ion. A sparser target orbital can be reached by a larger number of partial waves of the electron in the continuum, which leads to a narrower Gaussian. Thus, it is natural to associate the wide and narrow Gaussians with two characteristic regions in the target coordinate space. In DPI of the 2s-shell atomic targets, these two regions are related to the positive and negative oscillations of the target orbital. In the present case of a 3s-shell target orbital, there are three oscillations but the first one, near the origin, is very small as is seen in figure 4b, where the Mg 3s orbital is compared to the He 1s one.

The di-gaussian function (6) has been fitted to the experimental data and CCC calculations. The obtained parameters for the experimental data (and the CCC calculations) are as follows: A_2/A_1= 0.42±0.08 (0.43), $\Delta\vartheta_1$= 30±2° (41.2), $\Delta\vartheta_2$=95±4° (89.2), φ = 133±5° (160). In comparison, the theoretical Gaussian width for He is 97° which is similar to the $\Delta\vartheta_2$ parameter of Mg. This is consistent with the similar peak positions of the negative oscillation of the Mg^+ 3s orbital and the positive oscillation of the He^+ 1s orbital, as shown in figure 4b. The comparison between the

theoretical and experimental di-Gaussian parameters is quite satisfactory. The experimental width $\Delta\vartheta_1$ tends to be smaller than the predicted one. Even though the di-Gaussian fringe is relatively insignificant in comparison with the central Gaussian peak, its contribution to the TDCS is actually dominant. This is shown in figure 2 where the TDCS at ϑ_1=0, 30 and 60° are plotted. At ϑ_1=0°, almost all of the intensity of the TDCS comes from the di-Gaussian fringe and almost none from the central Gaussian peak. The Gaussian contribution becomes more significant at the other fixed angles ϑ_1=30 and 60°, but the di-Gaussian fringe still dominates the TDCS. This behavior can be easily understood because the Gaussian peak at ϑ_{12}=180°, which corresponds to the back-to-back emission, is suppressed by the kinematic factor due to the dipole selection rules, while the di-Gaussian fringe is away from the kinematic node and its contribution is not damped.

In the case of unequal energy sharing, both the gerade and ungerade amplitudes contribute to the measured TDCS. Bolognesi et al [38] in 2003 proposed a procedure that allows to extract the moduli and relative phase of the a_g and a_u complex amplitudes from the experimental data. The method does not rely on any approximation, needs only three determinations of the TDCS at the same relative angle ϑ_{12} between the photoelectrons and can be applied to any set of experimental data. The method, when applied to measurements with linearly polarized incident radiation, leaves undetermined the sign of the relative phase between the gerade and ungerade complex amplitudes [38]. When two sets of measurements with linearly and circularly polarized radiation are combined, this allows also the sign of the phase to be determined [39]. Here we apply the method to the measurements reported in Figures 3. Having four determinations of the TDCS (the two complementary cases differ only by the sign in front of the second addendum in eq. (3)) the method by Bolognesi *et al.* [38] can be applied to four different combinations of the measurements. To check the consistency of the results, the method has been applied to two combinations and the results averaged. The results for the amplitudes are shown in figure 5, where also the predictions by CCC are reported

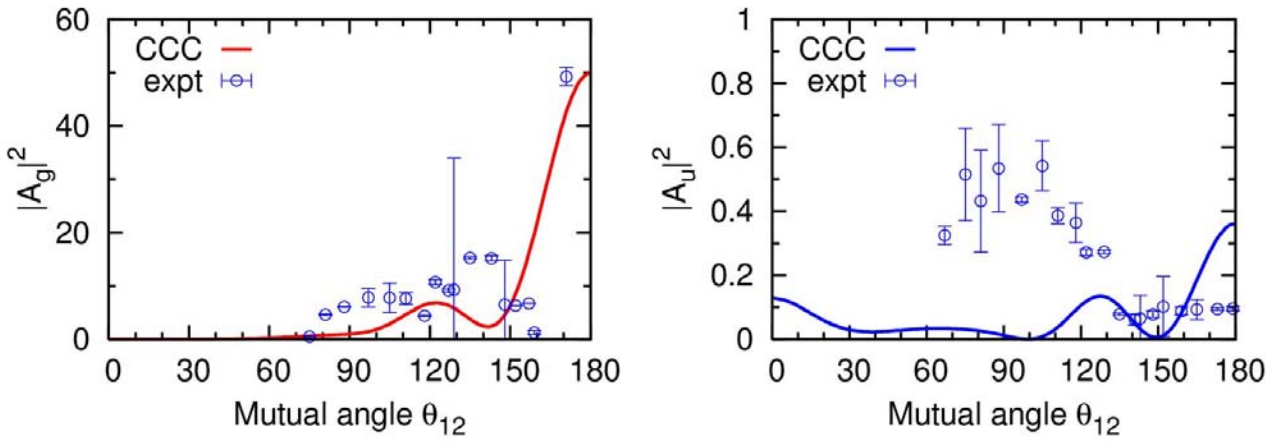

Figure 5: The symmetric gerade and ungerade amplitudes for the unequal energy sharing (E_1=10.4 eV, E_2=22.4 eV). The full CCC calculation is represented by the solid line

The comparison between the CCC calculated and experimental amplitudes is quite satisfactory in the case of the symmetric gerade amplitude. The ungerade amplitude is predicted to be one order of magnitude smaller than the gerade one and the experimental measurement agrees with this prediction, however the experimental values are smaller than the theoretically predicted ones at ϑ_{12}=180° and larger in the region about ϑ_{12}=90°. Considering the absolute values of the two amplitudes and the quality of the present measurements, the intensity and shape of the ungerade amplitude in the present kinematics might be too small to be reliably determined. These differences in the calculated and experimentally derived amplitude may also explains the differences observed in the unequal energy sharing TDCS at ϑ_1=0° (Figures 3). The small value of the ungerade amplitude also explains why the shape of the complementary kinematics are not too different., These findings are consistent with the ones in He. Indeed the analysis of the symmetrised amplitudes reported by Kheifets and Bray[36] at a few excess energies from 9 to 60 eV and several energy sharing ratios R=E_1/E_2 showed that the contribution of the a_u amplitudes becomes significant only at high excess energy and large R.

C. TDCS with ϑ_1=90°

Previous measurements of DPI in alkaline-earth-metal atoms have shown that the most intriguing results are obtained when the fixed electrons is detected at ϑ_1=90° with respect to the direction of the polarization of the incident radiation in both the equal and unequal energy sharing condition. In the case of Ca, the TDCS measured by Ross et al. [18] in the region of the Ca 3p→3d resonances

displayed two pairs of lobes in both the equal and unequal energy sharing kinematics. This is in contrast with the single pair observed in the TDCS of He. In the case of Sr the TDCS measured by West et al. [20] and Sheridan et al.[21] in the region of the 4p→4d resonance showed a non-zero value for antiparallel ejection of the two electrons (ϑ_{12}=180°). This particular kinematics cannot be accessed with our present set-up, thus here we have performed a simulation and analysis of the TDCs that can be expected on the ground of the experimental and theoretical results presented in Section III.

First of all, the theoretical predictions for the equal energy sharing case (figure 6a) clearly show that the TDCS at ϑ_1=90° displays two pairs of lobes. A comparison between the two CCC calculations with and without the resonance effect proves that the effect of the resonance is to enhance the inner lobes, but the number of lobes is due to the initial state wavefunction. A four lobe structure is also predicted for the unequal energy sharing conditions (figure 6b and c) where the small value of the a_u amplitude makes the complementary TDCS very similar. These results are consistent with the observation of two pair of lobes in the case of Ca [18] and clearly identify them as due to the target orbital wave function and not to an effect of the resonance.

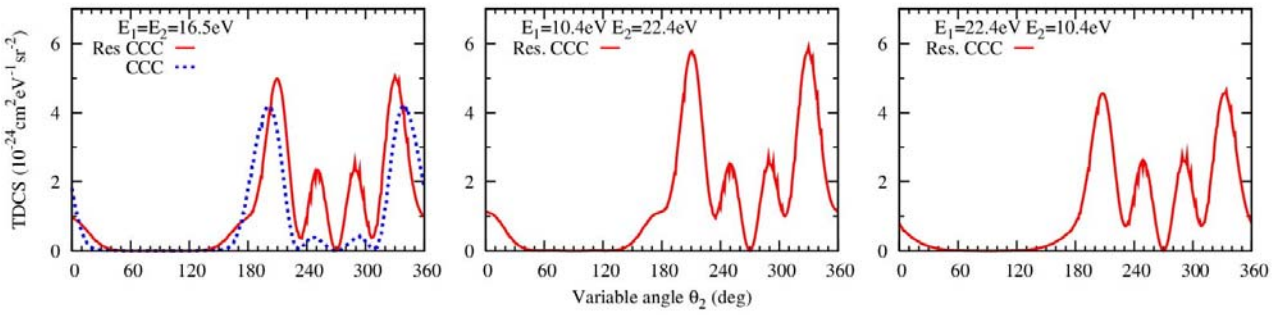

Figure 6 : (*left panel*) The TDCS in equal energy sharing condition at ϑ_1=90° calculated by CCC with (solid red line) and without (dotted blue line) the inclusion of the resonance effect. (*central panel*) the TDCS in unequal energy sharing condition (E_1=10.4 eV, E_2=22.4 eV) and ϑ_1=90° calculated by the CCC (*right panel*). As in the central panel but E_1=22.4 eV and E_2=10.4 eV.

Now, let us consider an experimental aspect typical of the TDCS measured near ϑ_1=90°. This is described by Figures 7 where the calculated TDCS in the equal energy sharing conditions at ϑ_1=0°, ±5° (figure 7a) and ϑ_1=90°,85°and 95°(figure 7b) using the parameters obtained in Section III from the fit to the a_g amplitude calculated by CCC are compared. A variation of 5° in ϑ_1 about ϑ_1=0° results in a change of the shape of the TDCS, with the relative intensity of the lobe at ϑ_{12}>180° increasing with respect to the one at ϑ_{12}<180° as ϑ_1 varies from -5 to 5°, and a shift in position. Qualitatively similar effects are observed when ϑ_1 varies from 85 to 95°. In both cases, a vanishing TDCS at ϑ_{12}=180° is observed, as expected by the symmetry selection rules of formula (4).

However, while in the case of ϑ_1=0° (figure 7a) the small size and large distance in relative position of the inner lobes preserve a full region of vanishing TDCS around ϑ_{12}=180°, this is not the case for the ϑ_1=90° case (figure 7b). In this latter case indeed the superposition of the three distributions produces a partial filling of the node at 270°, i.e. ϑ_{12}=180° with respect to ϑ_1=90°.

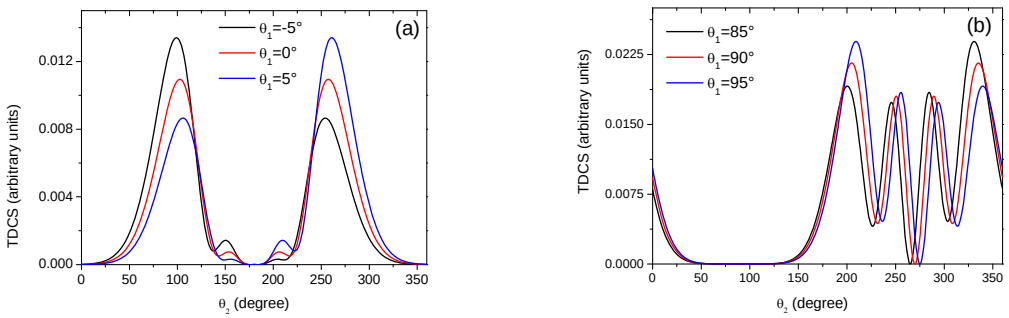

Figure 7 : TDCS for the equal energy sharing calculated using the parameters form the fit to the CC calcualtions (see text) for ϑ_1=-5°,0°,5° (a) and ϑ_1=85°,90°,95° (b).

Now when the experimental angular acceptance is taken into account in the simulation, no significant changes in the shape of the TDCS are produced in the ϑ_1=0° case (figure 8a), while an evolution of the shape of the cross Section is observed in the ϑ_1=90° case and a filling of the node at ϑ_{12}=180° can be achieved. This is illustrated in figure 8b where the TDCS calculated for several ϑ_1 acceptances (0°<FWHM<20°) are shown. Vice versa, the inclusion of a finite ϑ_2 acceptance does not produce appreciable changes in the shape of the simulated TDCS.

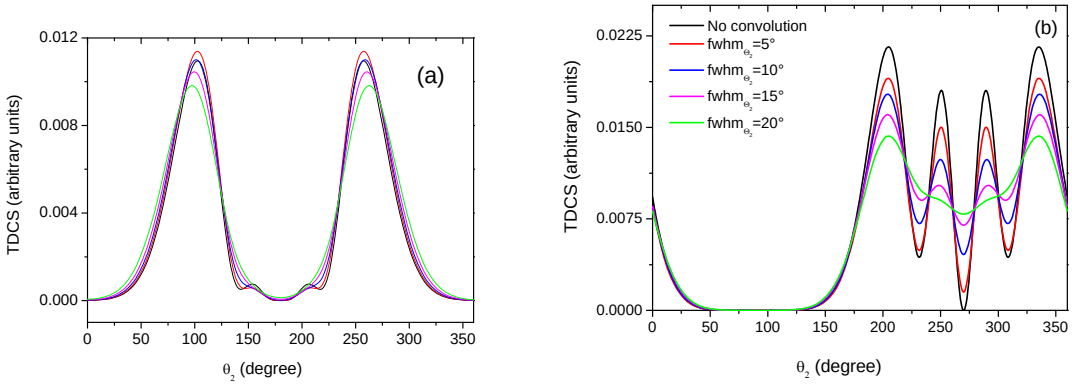

Figure 8: Convolution of the TDCS calculated as in Figure 7 by the angular acceptances ϑ_1 of the fixed electron.

Figures 7b and 8b clearly prove that the TDCS measured at ϑ_1=90°can suffer of instrumental effects, which may mask or alter the real shape of the TDCS.

Now, under the approximation that a di-gaussian parametrization can be used also in the case of the double photoionization of Sr to Sr^{2+} ($5s^{-2}$) state, the TDCS for the equal energy case at about 8 eV above threshold has been simulated. In the simulation, we have taken into account that the Gaussian function becomes narrower as the atomic number of the alkaline earth increases and the excess energy decreases [11]. The calculated TDCS with $\Delta\vartheta_1$= 20°, $\Delta\vartheta_2$= 85°, φ = 160° and FWHM=15° in ϑ_2 for several values of the A_2/A_1 ratio are shown in figure 9. The ure shows that there are conditions where a peak at ϑ_{12}=180° appears in the TDCS.

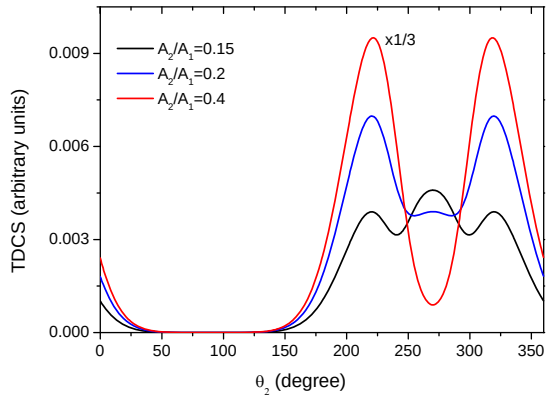

Figure 9. Simulation of the TDCS at E_1= E_2=8 eV with $\Delta\vartheta_1$= 20°, $\Delta\vartheta_2$= 85°, φ = 160° and FWHM=15° in ϑ_2 for several values of the A_2/A_1 ratio

The TDCS reported in figure 9 for $A_2/A_1 \leq 0.2$ might in principle explain the observation reported in the case of Sr [20,21]. However, the approximation of a di-gaussian amplitude also for the Sr gerade amplitude, the guessed A_2/A_1 ratio and the arbitrary parameters used for the convolution in ϑ_1 and ϑ_2 do not allow to state that instrumental effects such as a finite angular acceptances, rather than violation of the symmetry selection rules, explain the filling of the back to back node at ϑ_1=90° observed in Sr. Nonetheless they set a claim for further measurements and calculations in this peculiar kinematics.

V. Conclusions

The TDCS of Mg at 55.49 eV have been measured in both equal (E_1=E_2=16.4 eV) and complementary unequal energy (E_1↔E_2=10.4↔22.4 eV) sharing kinematics. The basic quantities which determine the double photoionization process, the symmetrised gerade and ungerade amplitudes and their relative phase, have been extracted from the experiment. The experimental

results have been compared with CCC calculations, which incorporate the effect of the 2p→3d resonant excitation. The calculations show that the resonance enhances the absolute cross Section and changes the relative intensity of some features, but it does not introduce extra feature in the TDCS.

The main result of the equal energy sharing is that the gerade amplitude displays fringes that cannot be represented by the Gaussian ansatz. The di-gaussian parameterization, introduced to take into account the radial oscillation of the target orbital [37,24], provides a better representation of the experimental amplitude.

In the case of the unequal energy sharing, a small value of the ungerade amplitude hampers its reliable extraction from the experimental TDCS. Nevertheless a general satisfactory agreement between the experimental TDCS and the CCC predictions has been found.

On the basis of the present findings, a simulation has been undertaken of the expected TDCS in equal energy sharing conditions when the fixed electron is detected at 90° with respect to the polarization of the incident radiation. We found that, firstly, in this kinematics two pairs of lobes are expected as observed in previous measurements on Ca and then a finite acceptance angle can lead to a TDCS with either a node or a peak at ϑ_{12}=180°. Due to the approximation used in the simulation we cannot state that these results solve the previous puzzling observations in the TDCS of Sr, but provide a warning and, at the same time, a stimulus for future theoretical and experimental studies of DPI in alkaline-earth-metal atoms.

Acknowledments

Work partially supported by the MIUR PRIN 2009W2W4YF and 2009SLKFEX. The authors thanks Paolo Bertoch and Federico Salvador for the prompt and qualified technical assistance in the assembling the Mg oven in the multicoincidence end-station of the gas phase Photoemission beamline at Elettra. Resources of the Australian National Computational Infrastructure Facility were used in this work.

References

[1] L. Avaldi and A. Huetz, J. Phys. B: At. Mol. Opt. Phys. **38,** S861 (2005)
[2] J. S. Briggs and V. Schmidt, J. Phys. B: At. Mol. Opt. Phys **33,** R1 (2000)
[3] L. Malegat, *Phys. Scr.* T **110,** 83 (2004)
[4] A.S Kheifets and I. Bray, Phys Rev. A **65**, 012710 (2002)
[5] F. Citrini, L. Malegat, P. Selles and A. K. Kazansky, Phys Rev. A **67**, 042709 (2003)
[6] J. Colgan and M.S. Pindzola, Phys Rev. A **65**, 022709 (2002)
[7] S.C. Ceraulo, R.M. Stehman and R.S. Berry, Phys Rev. A **49**, 1730 (1994)
[8] A. Kazansky and V.N. Ostrovsky, J. Phys B: At. Mol. Opt. Phys. **30**, L835 (1997)

[9] F. Maulbetsch, I.L. Cooper and A.S. Dickinson, J. Phys B: At. Mol. Opt. Phys. **34**, L119 (2000)
[10] L. Malegat, F. Citrini, P. Selles and P. Archirel, J. Phys B: At. Mol. Opt. Phys. **33**, 2409 (2000)
[11] A.S. Kheifets and I. Bray, Phys Rev. A **75**, 042703 (2007)
[12] A. S. Kheifets, I. Bray, J. Colgan J and M. S. Pindzola J. Phys. B: At. Mol. Opt. Phys. **44**, 011002 (2011)
[13] R. Wehlitz, D. Lukić and J.B. Bluett, Phys Rev. A **71**, 012707 (2005)
[14] R. Wehlitz, P.N. Juranić and D.V. Lukić, Phys Rev. A **78**, 033428 (2008)
[15] R. Wehlitz, P.N. Juranić, Phys Rev. A **79**, 013410 (2009)
[16] T. Osawa, Y. Tohyama, R. Kobayashi, S. Obara, Y. Azuma and T. Nagata , XIV International Conf. on VUV Rad. Phys., Cairns, Australia, (2004) p. W-P0-28
[17] H.-J. Beyer, J.B. West, K.J. Ross and A. De Fanis, J. Phys B: At. Mol. Opt. Phys. **33**, L767 (2000)
[18] K.J. Ross, J.B. West and H.-J. Beyer, J. Phys B: At. Mol. Opt. Phys. **30**, L735 (1997)
[19] K.J. Ross, J.B. West, H.-J. Beyer and A. De Fanis, J. Phys B. At. Mol. Opt. Phys. **32**, 2927 (1999)
[20] J.B. West, K.J. Ross, H.-J. Beyer, A. De Fanis and H. Hamdy, J. Phys B. At. Mol. Opt. Phys. **34**, 4167 (2001)
[21] P. Sheridan, M. Grimm and E. Sokell, J. Phys B. At. Mol. Opt. Phys. **41**, 165204 (2008)
[22] M Ya Amusia, V A Kilin, A Ehresmann, H Schmoranzer and K -H Schartner J. Phys. B: At. Mol. Opt. Phys. **26**, 1281 (1993)
[23] A. S. Kheifets and I. Bray, Phys. Rev. A**75**, 042703 (2007).
[24] E. Sokell, P. Bolognesi, A. Kheifets, I. Bray, S. Safgren and L. Avaldi, Phys. Rev. Lett. **110**, 083001 (2013)
[25] P. Bolognesi *et al*, J. Electron. Spectrosc. Rel. Phenom. **141**,105 (2004)
[26] R.R. Blyth *et al*, J. Electron Spectr. Rel. Phenom. **101-103**, 959 (1999)
[27] S.H. Soutworth, A.C. Parr, J.E. Hardis, J.L. Dehmer and D.M.P. Holland, Nucl. Instrum. Meth. A **246**, 782 (1986)
[28] B. Kämmerling, A. Hasumann, J. Laüger and V. Schmidt, J. Phys. B : At. Mol. Opt. Phys. **25**, 4773 (1992)
[29] P. Bolognesi *et al.* J. Phys. B: At. Mol. Opt. Phys. **34**, 3193 (2001)
[30] K.J. Ross and J. West, Meas. Sci. Technol. **9**, 1236 (1998)
[31] M. Y. Amusia and A. S. Kheifets, Phys. Lett. A **82**, 407 (1981)
[32] M.Stener, G.De Alti , G. Fronzoni and P. Decleva, Chem. Phys. **222**, 197 (1997)
[33] U. Fano, Phys. Rev. **124**, 1866 (1961)
[34]P. Bolognesi et al., Physica Scripta T110, 62 (2004)
[35] A. R. P. Rau, J. Phys. B9, L283 (1976), J. M. Feagin, J. Phys. B17, 2433 (1984), J. M. Rost, J. Phys. B27, 5923 (1994).
[36] A. S. Kheifets and I. Bray , Phys. Rev. A**65**, 022708 (2002)
[37]A. S. Kheifets, I. Bray, J. Colgan J and M. S. Pindzola J. Phys. B : At. Mol. Opt. Phys. **44**, 011002 (2011)
[38] P. Bolognesi , A. S. Kheifets , I. Bray , L. Malegat, P.Selles , A.K. Kazansky and L. Avaldi , J. Phys. B: At. Mol. Opt. Phys. **36**, L241 (2003)
[39] P. Bolognesi, V. Feyer, A. Kheifets, S. Turchini, T. Prosperi, N. Zema and L. Avaldi, J. Phys. B: At. Mol. Opt. Phys. **41**, 051003 (2008)